Spring 1996

Frequency Response Enhancement of a Flow Sensor Using Diamond Thin Films Synthesized by Plasma CVD

John Curren Hagwood
Old Dominion University

FREQUENCY RESPONSE ENHANCEMENT OF A FLOW SENSOR USING DIAMOND THIN FILMS SYNTHESIZED BY PLASMA CVD

by

John Curren Hagwood
B.S.E.T. May 1993, Old Dominion University

A Thesis Submitted to the Faculty of
Old Dominion University in Partial Fulfillment of the
Requirements for the Degree of

MASTER OF SCIENCE

ELECTRICAL ENGINEERING

OLD DOMINION UNIVERSITY
May 1996

Approved by:

Sacharia Albin

Vishnu Lakdawala

Linda Vahala

ABSTRACT

FREQUENCY RESPONSE ENHANCEMENT OF A FLOW SENSOR USING DIAMOND THIN FILMS SYNTHESIZED BY PLASMA CVD

John Curren Hagwood
Old Dominion University
Director: Dr. Sacharia Albin

Theoretical modeling conducted previously in our Microelectronics Laboratory has shown that a layer of diamond film inserted between a metal film and a substrate will enhance the frequency response of a conventional thin film flow sensor. This thesis involved fabricating and testing a conventional thin film sensor of nickel on quartz (Ni/Q) and a diamond enhanced sensor (Ni/D/Q) for comparative frequency response analysis to validate the theory. Diamond films were grown onto quartz substrates using a microwave plasma enhanced chemical vapor deposition process. Conditions were established to synthesize continuous diamond films on quartz substrates. These films were characterized by scanning electron microscopy and Raman spectroscopy. The frequency response of the Ni/Q and Ni/D/Q sensors were measured using a constant temperature anemometer. The diamond enhanced sensor yielded a frequency response of 240 kHz compared to 100 kHz for the conventional thin film sensor, which is in agreement with the theoretically predicted results.

ACKNOWLEDGMENTS

I would like to honor God and his Son Jesus Christ for imparting unto me the opportunity and stamina to accomplish this worthwhile goal.

I am deeply grateful to Dr. Sacharia Albin for his leadership, patience and understanding throughout this research, without whom this work would not have been possible. I would also like to extend gratitude to Dr. Vishnu Lakdawala and Dr. Linda Vahala for their willingness to serve on my committee and review my thesis.

I would also like to acknowledge Bhaskar Bulusu, Arnel Lavarias, Jianli Zheng, Weihai Fu, Melanie Ratcliff, Charles Cole, Todd Lindley and Willie Bowen for making the past three years enjoyable, as well as educational. Special thanks go to Mike Adams and Dr. John Cooper for their assistance with SEM and Raman Spectroscopy, respectively .

I am very grateful to Scott Martinson, Michael Scott, David Gray and Jim Bartlett of NASA Langley for the many technical discussions. I would like to acknowledge with gratitude the fellowship awarded through the NASA Graduate Researchers Program, under contract number NGT-70307. Also, I acknowledge the assistance provided through the Virginia Space Grant Consortium Aerospace Graduate Research Fellowship.

Finally, I honor my lovely wife, Linda, and my beautiful daughter, Cynthia, for providing their love and inspiration. Lastly, Mom and Dad thanks for your constant support and belief in my abilities.

TABLE OF CONTENTS

PAGE

LIST OF TABLES

LIST OF FIGURES

CHAPTER 1

INTRODUCTION

Technological advances in aerospace research and development have produced aircraft vehicles whose normal operating speeds are in the supersonic and hypersonic regime. Specific examples of these advances include the hypersonic research aircraft (NASA X-15), the French-British Concorde and the space shuttle. High speed flight applications, such as these, are known to generate excessively turbulent boundary layers and aerodynamic heating along the aircraft. Detecting the origin and development of these boundary layers at high temperatures is a critical aspect of aerodynamic research. Therefore, a need exists for a device with properties which will correctly measure these flow characteristics. It has been shown recently that non-intrusive measurements in high velocity flow regions can be achieved through laser-doppler velocimetry [1]. Miles et al. [2] also reported on studying turbulent structures in high speed flows to obtain instantaneous images of the velocity profile using a newly developed laser induced fluorescence method. An inherent problem in both of these methods is that neither can be used in continuous turbulent measurements. However, thermal anemometers have emerged as one of the few instruments which can serve the purpose of obtaining data continuously under turbulent flow conditions. These devices incorporate flow sensors for

intrusively measuring the thermal energy transferred by convection to a surrounding fluid. The flow sensors are designed either in the form of a wire or a thin film. The thin film sensors are deposited onto an insulating substrate which makes them mechanically strong and durable. The surface area to mass ratio is large for thin film sensors; hence they have large signal to noise ratio. Therefore, the transient response should be better, and these sensors are useful in high frequency applications. In order to clearly understand the need for such sensing capabilities, a brief review of the relevant flow properties is given, followed by previous work done with thin film anemometers.

1.1 Types of Flows

The state of real fluid flow can be classified as being laminar, turbulent, or in laminar-turbulent transition. This classification is made according to a dimensionless quantity known as the Reynolds number, represented by,

$$Re = \frac{v\rho L}{\eta} \qquad (1)$$

where v is the flow velocity, ρ is the fluid density, L is the characteristic linear dimension and η is the fluid viscosity. Laminar flow is a condition in which the fluid moves in layers without fluctuations or turbulence. As a result, successive particles passing the same point have the same velocity. In contrast, turbulent flow is a situation in which the particles of the fluid move in a disordered manner and in irregular paths. This chaotic condition results in an exchange of energy and momentum from one portion of a fluid to another. Under certain conditions, the presence of laminar and turbulent flow states may occur

simultaneously. In this case, a laminar-turbulent transition region develops between the laminar and turbulent flow. The formation of this transition region in the presence of a flat surface is discussed in the next section.

1.2 Boundary Layers

Figure 1 illustrates the fluid flow states corresponding to the velocity boundary layer development over a flat surface. For flow over any surface, there will always exist a velocity boundary layer and hence surface friction [3]. The velocity boundary layer represents the region in which the velocity components differ between the surface and the freestream. The surface friction coefficient, C_f, a dimensionless parameter which depends on the surface shear stress, can be expressed as,

$$C_f = \frac{\mu}{\rho u_\infty^2} \frac{\partial u}{\partial y}\Big|_{y=0} \tag{2}$$

where μ is the dynamic viscosity, u_∞ is the free stream velocity, ρ is the density, and the partial derivative is the velocity gradient at the surface. If the dynamic viscosity, free stream velocity and fluid density are known the skin friction coefficient can be determined by measuring the change in the normal velocity component. The velocity boundary layer is created in the following manner. A free stream velocity with components u and v are incident upon the leading edge of a flat-plate surface. At the plate surface, the velocity components are zero due to retardation caused by the surface shear stresses. These shear stresses further impose a retardation effect such that a velocity boundary layer thickness, $\delta(x)$, is created. The initial velocity boundary layer is due to laminar flow and grows with

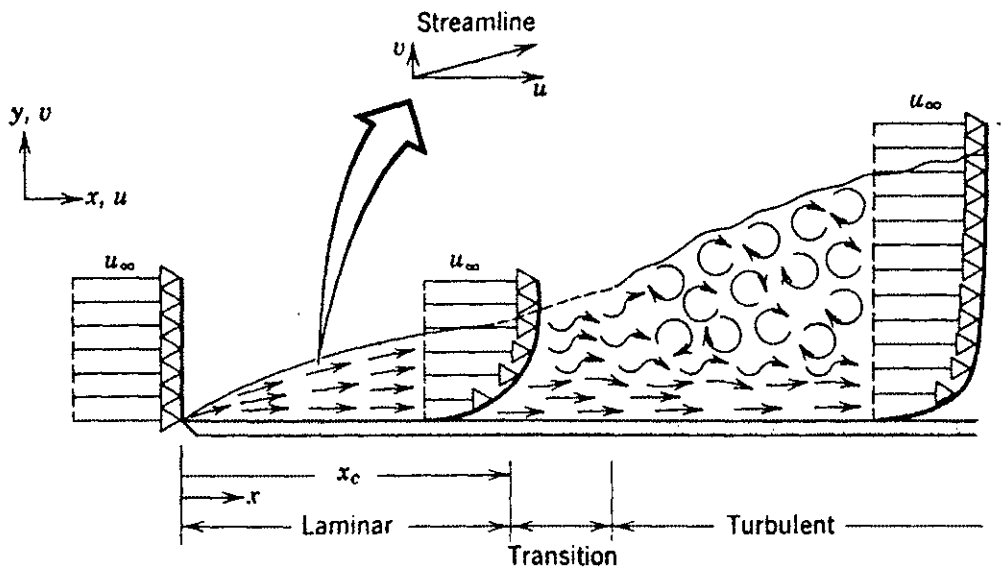

Figure 1: Velocity boundary layer created with three regions of flow characteristics: laminar, laminar-turbulent transition, and turbulence [3].

an approximately parabolic velocity profile. In the laminar region, the horizontal component, u, is much greater than the transverse component, v. The laminar-turbulent transition region begins developing as the transverse velocity components increase. The distance at which the transition from laminar to turbulence occurs is known as the critical Reynolds length, x_c, and from which the critical Reynolds number is determined using equation 1. Beyond the critical Reynolds length the transverse components of the fluid are further amplified, and as a result turbulence occurs. Several factors which influence the velocity boundary layer formation are surface roughness, pressure, and Reynolds number. Laminar-turbulent transitions develop faster for surfaces which are not very smooth. Also, high Reynolds number flows will be turbulent even when very smooth surfaces are incident upon.

A thermal boundary layer develops if the surface temperature is different from the fluid flow. The Nusselt number is a dimensionless parameter which gives the ratio of the convective heat transfer to conduction occurring at the surface expressed as,

$$Nu = \frac{hL}{k_{fl}} \tag{3}$$

where h is the heat transfer coefficient, L is the characteristic linear dimension and k_{fl} is the thermal conductivity of the fluid. The value of the Nusselt number is a function of both the Reynolds number and a dimensionless quantity known as the Prandtl number. The Prandtl number is a ratio of the momentum diffusivity to the thermal diffusivity in the

boundary layers given as,

$$Pr = \frac{c_p \mu}{k} \tag{5}$$

where c_p, μ, and k are the specific heat capacity, dynamic viscosity, and thermal conductivity, respectively. By computing the Nusselt value for a given fluid, the heat transfer coefficient can be determined. The fact that the Nusselt number is a function of both the Reynolds and Prandlt number implies that the rate of heat transfer corresponds to the velocity components of the fluid. At the interface of the surface and the fluid heat transfer occurs by diffusion since the velocity components are assumed zero. As the boundary layer thickens, the bulk motion of the fluid dominates the heat transfer. Therefore, measuring certain properties like skin friction and heat transfer provides useful information regarding the boundary layer.

Measuring boundary layer transitions is important for verifying computational fluid dynamic (CFD) code. CFD is a computer simulation routine which theoretically predicts how various flow parameters will affect an aircraft while in flight. This is useful in designing aircraft which can withstand different flow conditions.

1.3 Thin Film Anemometers

The idea of thin film anemometers dates back to work done by Lowell in the 1940's [4]. Thin metal films were initially studied as sensor elements due to their large temperature coefficient of resistance [5]. Bellhouse and Schultz [6] measured the mean

and dynamic skin friction by utilizing a heated thin film and a constant temperature anemometer. Thin films made of a platinum-silver alloy which were approximately 1μm thick were used as the sensing element. For skin friction measurements, the amount of heat transferred through convection was determined by the change in the electrical power supplied to the thin film. As a result, the voltage variation on the heated film corresponded to the turbulent fluctuations in the boundary layer. These experiments were conducted at low speeds ($Re \approx 10^4$) with a zero pressure gradient and the frequency response was limited to 100 Hz. This work was further verified through theoretical calculations and experimental testing by Brown [7]. His contribution was in demonstrating skin friction measurements with a heated film in the presence of a pressure gradient at low speeds. For both of these experiments, the thin films were either painted or soft baked onto an insulating substrate. A more preferred technique for sensor fabrication is through the use of modern vacuum deposition technologies. These techniques have the advantage of maintaining a controlled composition and permitting high quality depositions of very thin films.

Recently, thin film sensors have been used in high speed flows for evaluating boundary layer transitions [8]. In this study, the author compared the frequency response of several commercially available hot-film probes while using a constant temperature anemometer. The results demonstrated that all these probes were limited to 100 kHz as the usable frequency range. Researchers at NASA Langley have fabricated thin film sensors of Cr and Ni metal deposited onto insulating substrates, which have been used at both ambient and cryogenic temperatures [9,10]. These sensor have been tested in wind

tunnels and in aircraft flight experiments. The frequency response of these sensors are limited to around 60 kHz. However, in the supersonic and hypersonic speed regimes, it is expected that the frequency components will be in the range from 200-400 kHz. The sensor is the limiting factor for measuring such high frequency components. Therefore, a need arises for identifying appropriate sensor materials and fabrication techniques for detecting flow transitions in a high velocity, high temperature environment.

1.4 Material Parameters

Several criteria should be satisfied to effectively design and fabricate a flow sensor for high temperature applications. The sensor film must have a temperature coefficient of resistance; this allows temperature changes to be interpreted through voltage fluctuations. A standard equation which defines the resistance as a function of temperature is given as,

$$R = R_0 \left[1 + \gamma(T-T_0) + \gamma_1(T-T_0)^2 + \gamma_2(T-T_0)^3\right] \tag{6}$$

In this equation R is the resistance at temperature T, R_0 is the initial resistance at T_0 and γ, γ_1, γ_2 represent the temperature coefficients of resistance. Also, a first order approximation of the temperature sensitivity is given by,

$$\frac{dR}{dT} = \gamma R_0 = \frac{\gamma \rho_0 L}{A} \tag{7}$$

where ρ_0, L, and A are the resistivity, length and cross-sectional area of the film,

respectively. Maximizing $\gamma\rho_0$ is considered an appropriate condition in the selection of thin film materials for an ideal flow sensor.

Another design aspect is effectively selecting sensor materials which will exhibit a high frequency response. Achieving a high frequency response requires the combination of a thin film material with a high thermal conductivity and a substrate material with a low thermal conductivity. This is discussed further in Chapter 2. Even though metals such as nickel, platinum, and chromium have been routinely used as the sensor element, another potential material is diamond which possesses a larger thermal conductivity.

1.4.1 Sensor Film Material

Table 1 gives a comparison between the thermo-physical properties of film materials which could possibly be used. Among solid state materials, diamond has the highest value of thermal conductivity, five times that of copper, at room temperature. It is the hardest material known and it is chemically inert at high temperatures. Diamond has a high intrinsic resistivity, due to its large bandgap; yet, it can be doped to have a range of values from 0.1-100Ω-cm [12]. Applications utilizing these and other properties have recently been reported in different areas on sensing: hydrogen [13], temperature [14], and flow [15]. For all these experiments, diamond thin films were prepared by chemical vapor deposition (CVD).

1.4.2 Growth Technology

The feasibility of growing diamond thin films at low pressures by various chemical

vapor deposition processes has been demonstrated [16-18]. In general two classifications of growth techniques can be made according to their energizing mechanism: thermally assisted and plasma assisted. By comparison, electrodeless plasma CVD eliminates the usual film contamination which occurs during the thermal process. In particular, plasma excitation at microwave frequencies have an advantage of maintaining a larger plasma density with higher energy electrons, more so than their RF counterparts [19]. In addition, the ability to grow uniform thin films with microwave plasma enhanced chemical vapor deposition (MPECVD) has been demonstrated [20].

1.4.3 Sensor Substrate Material

The primary reason for choosing a substrate material is to ensure a high frequency response by maintaining a large ratio of the thermal conductivity of the film, k_f, to the substrate, k_s. Among the materials listed in Table 1, quartz has the lowest value of thermal conductivity. By comparison of the thermal conductivity values, the diamond/quartz combination has the highest ratio of film-to-substrate. However, the choice of quartz represents a disparity between the coefficient of thermal expansion (CTE) between the film and substrate. The coefficient of thermal expansion represents the change in the atomic spacing of a material when heated. This is important particularly in thin film processing where substrate temperatures routinely exceed 300°C. Under ideal conditions, the coefficient of thermal expansion between the film and substrate would be identical. However, none of the substrate materials meet the requirements of a large film-to-substrate thermal conductivity ratio and matching coefficients of thermal expansion.

Table 1: The thermo-physical properties of selected film and substrate materials.

Material	Thermal Conductivity k(W/m·K)	Coefficient of Thermal Expansion CTE($°C^{-1}x10^{-6}$)	Temperature Coefficient of Resistance TCRγ ($°C^{-1}x10^{-3}$)
Films			
Ni	90.7	13	6.7
Pt	71.6	9	3.926
Diamond	2300	0.8	-360
Substrates			
Al_2O_3	36	8.4	-
Quartz	10.4	12	-
Sapphire	46	8	-
Si	148	3	-

Hence, a compromise is made for preserving the frequency response. Furthermore, using quartz substrates in thin film processing has been demonstrated [21].

As a result, a flow sensor with a semiconducting diamond film on a quartz substrate should be ideal. However, theoretical studies have shown that an intermediate layer of diamond film between a metal film and a substrate can reduce the temperature of the metal film, when stimulated by x-ray pulses of nanosecond durations [22]. Consequently, the effective thermal conductivity of a metal film can be increased by an interlayer of diamond film between the metal and substrate.

1.5 Thesis Motivation

Conventional flow sensors are fabricated by depositing metal films directly onto insulating substrates and can measure instabilities up to 100 kHz. The motivation of this thesis research is to experimentally determine the effect on the frequency response of a sensor with a thin film of diamond inserted between the metal film and substrate. Comparative frequency measurements between a conventional sensor and the proposed diamond enhanced sensor are required. Results of theoretical studies of the frequency response of the two sensors are given in Chapter 2. For the diamond enhanced sensor, the nucleation and growth techniques for achieving uniform thin films on quartz substrates must be established, as discussed in Chapter 3. Thin metal film sensors must be patterned and deposited onto both quartz and diamond-on-quartz substrates. The fabrication technique and the testing procedure used for obtaining the frequency response are discussed in Chapter 4. The results of diamond film growth studies and frequency

measurements of the sensors are given in Chapter 5. Finally, a summary and conclusion of this research work is given in Chapter 6, along with suggested future work.

CHAPTER 2

THEORY OF SENSOR FREQUENCY RESPONSE

Theoretical analysis of the heat transfer characteristics is an important aspect for designing thin film sensors for high frequency applications. The transient response of the sensor is very complicated due to the different modes of energy transfer. However, it is known that the thermal diffusivity, α (m^2/s), is the controlling transport property for transient diffusion [3]. Therefore, it is necessary to obtain expressions which give the relationship between the thermal diffusivity and the transient response of a thin film sensor. Theoretical solutions of the heat diffusion equation have been done for a thin film sensor with planar geometry by Vidal [23]. The details of these theoretical calculations will be given. Bulusu [24] used computer simulations for solving the heat diffusion equation by implementing the finite difference method. These results give numerical values of the frequency response for both a conventional and a proposed diamond enhanced sensor. Finally, an analytical expression for the effective thermal diffusivity of a two layer system developed by Albin et al. [20] will be discussed.

2.1 Theoretical Calculations

An illustration of the sensor model used in Vidal's [23] research is shown in

Figure 2. A one-dimensional analysis was done for deriving both exact and approximate solutions for the structure. By considering the time dependent rate of heat transfer from the film, which has a thickness d, to the substrate, the following heat diffusion equations can be written,

$$\frac{\partial T_f}{\partial t} = \frac{k_f}{\rho_f c_f}\frac{\partial^2 T_f}{\partial y^2} \tag{8}$$

from $0 \le y \le d$ for the film and

$$\frac{\partial T_s}{\partial t} = \frac{k_s}{\rho_s c_s}\frac{\partial^2 T_s}{\partial y^2} \tag{9}$$

from $d \le y \le \infty$ for the substrate.

In these two equations, t represents time and T is the increment of temperature at t=o; k, ρ, and c, with subscripts f and s are the thermal conductivity, density and specific heat for the film and the substrate, respectively. The boundary conditions are given as,

$$t \le 0,\ T_f(y) = 0,$$

$$t > 0,\ y = 0,$$

$$\frac{\partial T_f}{\partial t}\Big|_{y=0} = \frac{-1}{k_f} q(t)$$

and,

$$t \le 0,\ T_s(y) = 0,$$

$$t > 0,\ y = d,\ T_f(d) = T_s(d),$$

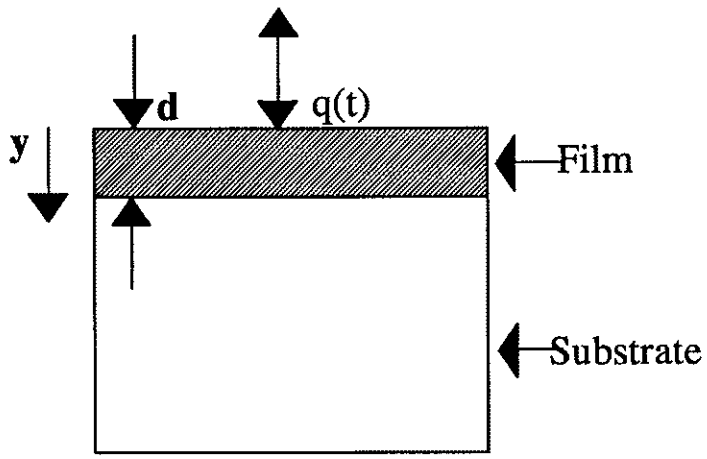

Figure 2: The sensor structure with planar geometry evaluated analytically where q(t) is the rate of heat conduction to and from the film.

$$k_f \frac{\partial T_f}{\partial t}\Big|_{y=d} = k_s \frac{\partial T_s}{\partial t}\Big|_{y=d}$$

$$\lim_{y\to\infty} T_s = 0$$

The term q(t) represents the rate of heat conduction to and from the film. Equations (8) and (9) are solved using Laplace transformations and the general expressions for the film and substrate temperature are given as,

$$T_f = \frac{1}{k_f}\sqrt{\frac{k_f}{\pi\rho_f c_f}}\int_0^t \frac{q(\lambda)}{\sqrt{t-\lambda}}\exp\left[\frac{-\rho_f c_f y^2}{4k_f(t-\lambda)}\right]d\lambda + \frac{1}{k_f}\sqrt{\frac{k_f}{\pi\rho_f c_f}}\sum_{n=1}^{\infty}\sigma^n \int_0^t \frac{q(\lambda)}{\sqrt{t-\lambda}} \left[\exp\left[\frac{-\rho_f c_f (2nd+y)^2}{4k_f(t-\lambda)}\right] + \exp\left[\frac{-\rho_f c_f (2nd-y)^2}{4k_f(t-\lambda)}\right]\right]d\lambda \quad (10)$$

for the film and,

$$T_s = \frac{1+\sigma}{k_f}\sqrt{\frac{k_f}{\pi\rho_f c_f}}\sum_{n=0}^{\infty}\sigma^n \int_0^t \frac{q(\lambda)}{\sqrt{t-\lambda}}\left[\exp-\frac{\left[(2n+1)d\sqrt{\frac{\rho_f c_f}{k_f}}+(y-d)\sqrt{\frac{\rho_s c_s}{k_s}}\right]^2}{4(t-\lambda)}\right]d\lambda \quad (11)$$

for the substrate where λ is the integration variable and σ is defined as,

$$\sigma = \frac{\sqrt{\frac{k_f\rho_f c_f}{k_s\rho_s c_s}}-1}{\sqrt{\frac{k_f\rho_f c_f}{k_s\rho_s c_s}}+1}$$

Now equations (10) and (11) represent the exact solutions for the temperature distribution. For high frequency analysis, the assumption is made that the substrate is infinitely thick and the thermal conductivity of the film is much larger than the substrate ($k_f \gg k_s$). This means negligible lateral heat transfer will occur between the film and the substrate. By also assuming the film thickness, d, and $\rho_f c_f$ are both very small the surface temperature, at y=0, is approximately the "average" film temperature. Therefore, equation (10) can be written as,

$$T_f = \frac{1}{k_f}\sqrt{\frac{k_f}{\pi\rho_f c_f}}\int_0^t \frac{q(\lambda)}{\sqrt{t-\lambda}}d\lambda + \frac{1}{k_f}\sqrt{\frac{k_f}{\pi\rho_f c_f}}\sum_{n=1}^{\infty} 2\sigma^n \int_0^t \frac{q(\lambda)}{\sqrt{t-\lambda}} \exp\frac{-n^2 d^2 \rho_f c_f}{4k_f(t-\lambda)}d\lambda \qquad (12)$$

The maximum frequency response is related to ($k_f/\rho_f c_f d^2$ or α_f/d^2) which is the inverse of the characteristic time in the exponential term. Therefore, choosing a thin film material with a large thermal conductivity value is sufficient for obtaining a high frequency response. As a result, the temperature changes in the film will be greater than in the substrate.

2.2 Numerical Calculations

Previous work in our group [24] to develop a computer model to solve the one-dimensional heat diffusion equation for the frequency response of a flow sensor has been done. The finite-difference method was used to analyze the two sensor models illustrated in Figure 3. The finite-difference form of the heat diffusion equation is given as,

$$\frac{\partial^2 T}{\partial x^2}\Big|_m \cong \frac{T(m+1,t) + T(m-1,t) - 2T(m,t)}{(\Delta x)^2} \tag{13}$$

for the second derivative and,

$$\frac{\partial T}{\partial t}\Big|_m \cong \frac{T(m-1,t) - T(m,t)}{\Delta t} \tag{14}$$

for the time derivative. The sensor is divided into a uniform mesh, separated by a spacing of Δx and a constant discretization time Δt. Substituting equations (13) and (14) into the heat diffusion equation yields the following,

$$T(m,t+1) = \frac{1}{M}[T(m+1,t) + T(m-1,t)] + [1 - \frac{2}{M}]T(m,t) \tag{15}$$

where,

$$M = \frac{(\Delta x)^2}{\alpha \Delta t}$$

Equation (15) was used during the simulation for determining the nodal temperatures. A sinusoidal forcing function was used to vary the surface temperature as follows,

$$T_s = T_0 + A\sin(\omega t) \tag{16}$$

where T_s is the surface temperature, T_0 is the initial temperature, and A is the amplitude of fluctuation. The temperature at the bottom of the substrate is assumed constant. Figure 4 illustrates the normalized amplitude response of the temperature variation for the two

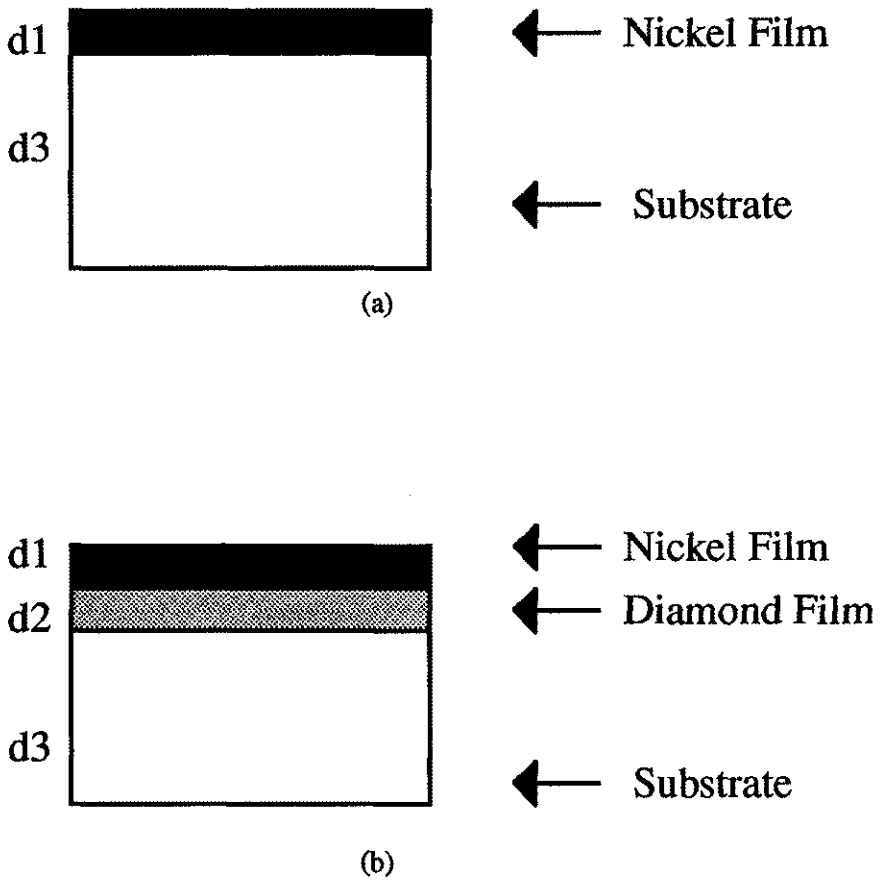

Figure 3: A schematic of the sensor models analyzed by finite-difference method
a) conventional metal film sensor, b) proposed diamond enhanced sensor.

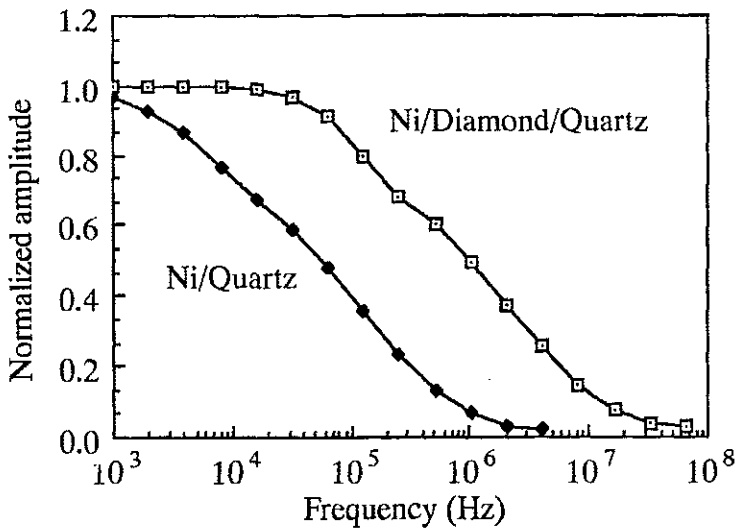

Figure 4: Theoretical frequency response of the two sensors calculated using the finite-difference method [25].

sensors. The 3dB response for Ni/Diamond/Quartz is around $3x10^5$ Hz. The response of the Nickel/Quartz structure is about an order of magnitude lower. This result numerically shows an intermediate layer of diamond will enhance the frequency response of a conventional metal film sensor.

2.3 Effective Diffusivity

Albin et al.[20] developed an analytical model to calculate the effective in-plane diffusivity of a two-layer system. For this experiment, diamond thin films were grown on silicon by MPECVD. A laser pulse technique was used to measure the thermal diffusivity of the diamond/silicon combination. These results demonstrated that an effective thermal diffusivity value of the diamond/silicon system was primarily a function of the thermal diffusivity or conductivity of the diamond. The analytical expression of the in-plane effective diffusivity value is given as,

$$\alpha_{eff}=\frac{\alpha_1\alpha_2(k_1d_1+k_2d_2)}{\alpha_2k_1d_1+\alpha_1k_2d_2} \tag{17}$$

In this expression α, k and d, with subscripts 1 and 2, represent the value of the thermal diffusivity, thermal conductivity, and thickness of the two layer system, respectively. For this experiment, the diamond films yielded a thermal conductivity value greater than type Ia. Figure 5 illustrates the variation of the effective diffusivity with the ratio of different thicknesses for a Ni/Diamond and a Ni/Quartz combination. The effective diffusivity value of the Ni/Diamond combination is primarily a function of the thermal

diffusivity of diamond when the ratio is less than 0.1. By comparison, the Ni/Quartz combination is approximately two orders of magnitude smaller. The results shown here further indicate the frequency response of the conventional sensor should be enhanced with an intermediate layer of diamond.

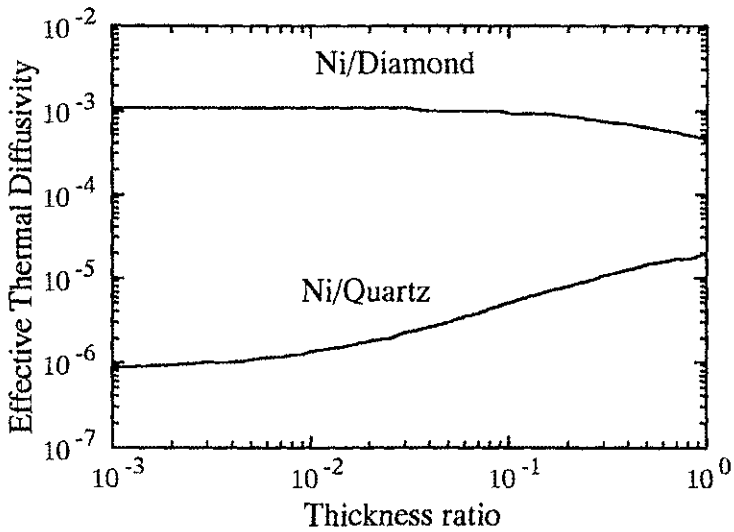

Figure 5: The variation of the effective diffusivity as a function of the thickness ratio between a Ni/Diamond and a Ni/Quartz combination [25].

CHAPTER 3

DIAMOND FILM SYNTHESIS

Establishing the nucleation and growth parameters for diamond deposition on quartz substrates is necessary before uniform thin film growth is possible. For this research, uniform growth is recognizable as a thin film which has a minimum surface roughness. It has been shown that surface abrasion and gas phase seeding are two techniques for increasing the nucleation density in diamond thin films [26,27]. Also, previous research has shown the ability to grow diamond thin films onto quartz substrates using CVD techniques [28,29]. In the following series of experiments several nucleation methods were investigated for determining the optimum technique for initiating the most stable nuclei during deposition. After this, the growth parameters were enhanced for providing uniform diamond thin films. This chapter covers these experiments through the following sections: substrate preparation, diamond system, and characterization methods.

3.1 Substrate Preparation

Quartz pieces of 1"x 1" squares were used as substrates in this work. These substrates were divided into three categories, according to the type of nucleation technique utilized. The first category consist of those substrates which received surface

abrasion as the only nucleation method. The second category was substrates which were nucleated through gas phase seeding alone. The third category involved those substrates for which surface abrasion and gas phase seeding were both done. This classification was done for investigating the effects of both nucleation methods, as well as determining which category of nucleation technique would yield the best uniformity of thin film growth. The technique utilized for the substrates in the first category is discussed in the next section, and the method for those mentioned in category two is deferred until section 3.2.1.

Surface abrasion is a pretreatment mechanism in which the substrate surface is intentionally abraded with either diamond particles or some other suitable material. A commercially available Minimet polishing tool was utilized for abrading the quartz surface. The schematic of the surface abrasion set-up is illustrated in Figure 6. SiC abrasive paper was first placed on a glass platen, which is normally positioned underneath the sample. The quartz pieces were attached to the substrate holder with a glue compound. Diamond paste was then added in between the SiC paper and the quartz substrate. The variable load arm was inserted into the top of the substrate holder. Once the polishing tool was activated, the variable arm moves the substrate in a predefined pattern. The applied downward force of the variable load arm was four pounds and the total time of abrasion was four minutes. After abrasion, the quartz pieces were detached from the substrate holder with toluene.

Each of the quartz substrates were cleaned prior to deposition. The cleaning procedure consisted of a ten minute deionized water rinse followed by fifteen minute ultrasonic rinse in acetone. Typically, the cleaning process is used to remove any

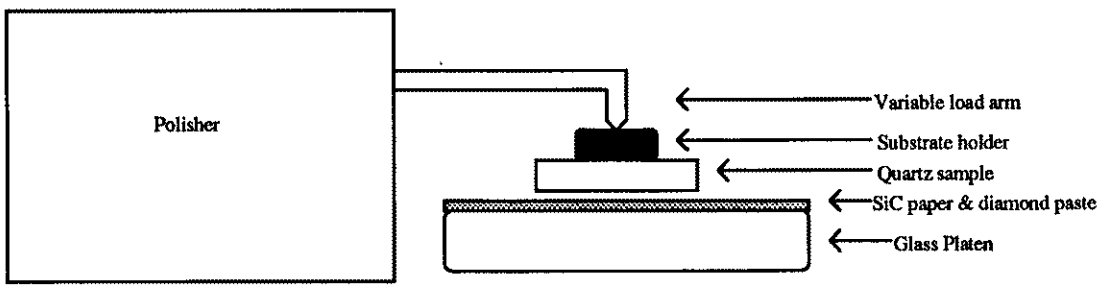

Figure 6: A schematic of the surface abrasion set-up using the Minimet polishing tool.

unwanted particles which have accumulated onto the substrate. This was especially effective in extracting the residual glue compound, which was present after detaching the substrates. Immediately following the cleaning routine, the quartz substrates were placed inside the deposition chamber.

3.2 Diamond Growth System

Diamond growth was done in the Microelectronics Laboratory at Old Dominion University using a high pressure microwave stainless steel (HPMS) Plasma-Enhanced Chemical Vapor Deposition system manufactured by ASTeX. Figure 7 illustrates a schematic of this deposition system. The deposition system consist of the following individual components: chamber, pumping system, pressure gauge, induction heater, gas sources, mass flow controllers, and microwave source. It is important to note that for this system diamond deposition occurs only after plasma stabilization is reached, which is discussed in the next section.

3.2.1 Deposition Set-up Procedure

The procedure for diamond growth began by evacuating the deposition chamber with the pumping system. The pumping system consists a turbomolecular pump backed by a vane pump, which collectively bring the deposition chamber pressure down from atmospheric to $<10^{-5}$ torr. The chamber pressure is measured using a capacitance manometer. After the chamber pressure reached vacuum level, the graphite susceptor was heated by a 3.5 kW induction heater to a predetermined temperature. The temperature of

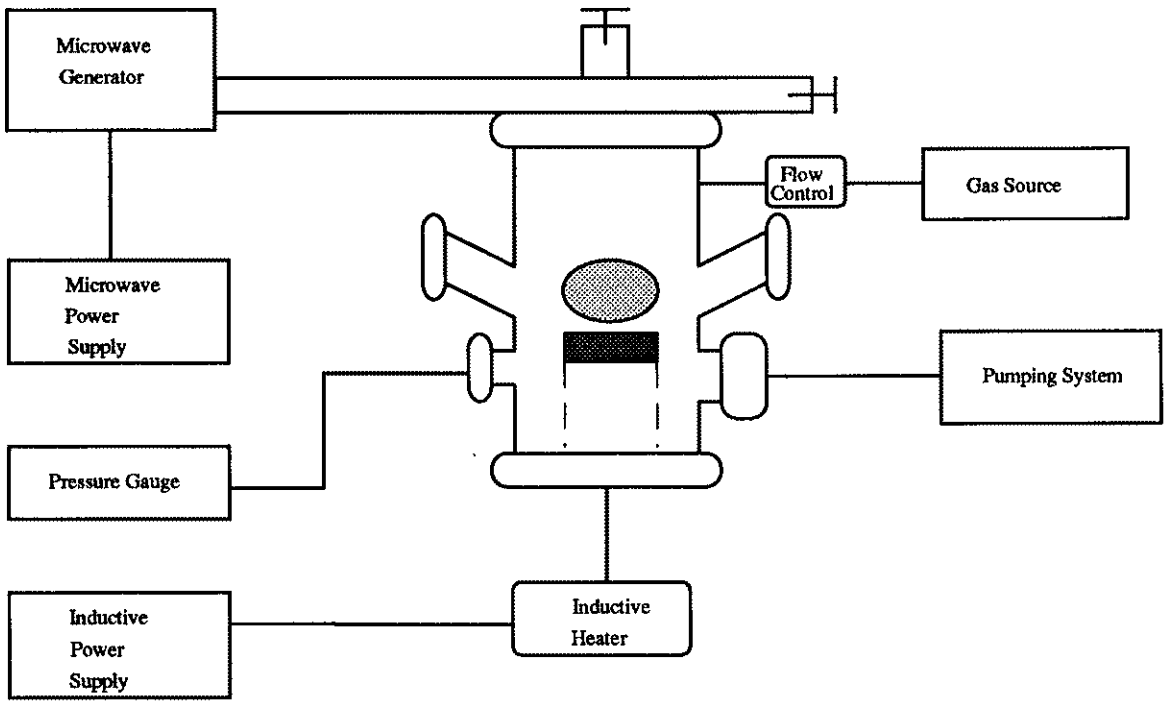

Figure 7: A schematic of the microwave plasma-enhanced chemical vapor deposition system for diamond growth.

the susceptor is monitored by a thermocouple. Once the desired susceptor temperature is obtained, hydrogen gas at a prescribed flow rate is admitted into the deposition chamber. A mass flow meter and flow controllers detect and control the gas flow rate, which is given in standard cubic centimeters (sccm). The chamber pressure was increased to 20 torr which is a recommended value for "striking" or creating the plasma. Finally, microwave power from a 1.5 kW continuous-wave (CW) power supply at 2.45 GHz was guided to the reactor. The formation of a purple ball located above the susceptor indicated when the condition of plasma stabilization was achieved. After achieving plasma stabilization, the nucleation and/or growth cycle began by introducing methane (CH_4) gas inside the chamber. It is important to note that after plasma stabilization, the difference between the nucleation and growth step is the deposition parameters used for each. Typical deposition parameters used are listed in Table 2.

The samples in category two were nucleated using a gas phase seeding method for increasing the nucleation density on quartz [29]. Experimentally, the method involved maintaining a high percentage of the methane/hydrogen gas ratio for a two hour time period. It is believed that this large ratio enhances the random formation of stable prenuclei carbon clusters, due to the high carbon concentration at the substrate surface [30]. For some of the experiments, the substrate temperature and the microwave power were also decreased during the seeding step. The growth step typically involved maintaining a methane/hydrogen gas ratio of 1%. The deposition time for growth was four hours when gas phase seeding was used and six hours for all others. In addition to

the hydrogen and methane gases routinely used, carbon monoxide was introduced during the growth cycle. The addition of carbon monoxide was to promote the formation of OH radicals within the gas phase. The formation of the OH radical has been shown to be effective in preferentially etching non-diamond growth [31].

3.3 Sample Characterization Techniques

Three characterization methods were used to evaluate the samples during different stages of the experiments. An optical microscope was used immediately following surface abrasion for investigating the uniformity of the abrasion technique. The microscope was also used to determine the lateral dimensions of the sensors, which are discussed in the next chapter. A Cambridge Stereoscan 100 Scanning Electron Microscope (SEM) was used for evaluating the uniformity and the surface morphology of the grown diamond films. Prior to SEM analysis some samples were sputter coated with a thin film Ag-Pd alloy to reduce surface charging. Figure 8 is a schematic of the experimental setup utilized for obtaining Raman measurements. The Raman spectra were measured with a Chromex spectrometer using the 514.5 nm line of an argon ion laser. The sample was placed at an angle with the incident laser light. Scattered light from the surface of the sample was collected with a 100x microscope objective. A lens was used to direct the collected light through a filter for removing any light corresponding to the incident laser wavelength. A second lens directed the filtered light to the spectrometer. The output of the spectrometer was analyzed by the computer and the corresponding light intensity values were plotted.

Table 2: Typical process parameters used during the nucleation and growth steps.

Deposition Parameter	Nucleation Step	Growth Step
Microwave Power (W)	723	1000
Substrate Temperature (^{o}C)	600	750-950
Hydrogen Flow (sccm)	430	900
Methane Flow (sccm)	70	9
Carbon Monoxide Flow (sccm)	0	0-27
Pressure (Torr)	20	35
Time (min)	0-120	240-360

The intensity values represented the shift in wavenumber from the incident light. The peak intensity values correspond to the different bonding states. Pure diamond (sp^3 bonding) exhibits a Raman peak at 1332 cm^{-1}; this represents the magnitude of the shift in wavenumber from the incident laser wavelength. Graphite and amorphous carbon (sp^2 bonding) have characteristic peaks at 1580 and 1500 cm^{-1}, respectively. Raman spectra for diamond growth using CVD techniques typically exhibits a peak at 1332 cm^{-1} with a broad band around 1550 cm^{-1} [26].

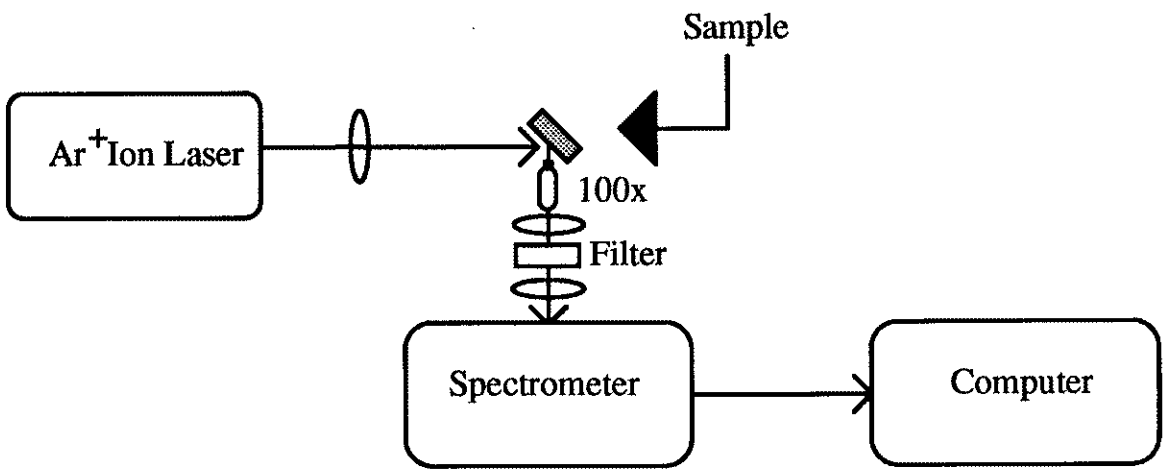

Figure 8: The experimental arrangement for Raman spectroscopy using an Argon ion laser.

CHAPTER 4

SENSOR FABRICATION & TESTING

Thin metal films are routinely deposited onto insulating substrates and used as sensor elements for analyzing the frequency response of certain transitions in fluid flow. Hot-film anemometry is a standard method of flow sensing which incorporates this type of sensor. Prior to actual flow testing, it is advantageous to estimate the cutoff frequency of a given sensor. Electrical signal testing is a technique for optimizing the frequency response of an anemometer system with a given sensor [32]. Therefore, this chapter discusses the fabrication technique, anemometer system and testing procedure used for the hot-film sensors in this research.

4.1 Sensor Fabrication

Figure 9 illustrates the cross-sectional and top view of the two sensor structures fabricated: nickel-on-diamond-on-quartz (Ni/D/Q) and nickel-on-quartz (Ni/Q). Thin nickel films were first deposited onto both quartz and diamond-on-quartz substrates by an electron beam evaporation technique, which uses thermal energy to vaporize and condense the thin film material to the surface of the entire substrate [33]. These films were used as the sensing material partly because of the resistivity and large temperature coefficient of

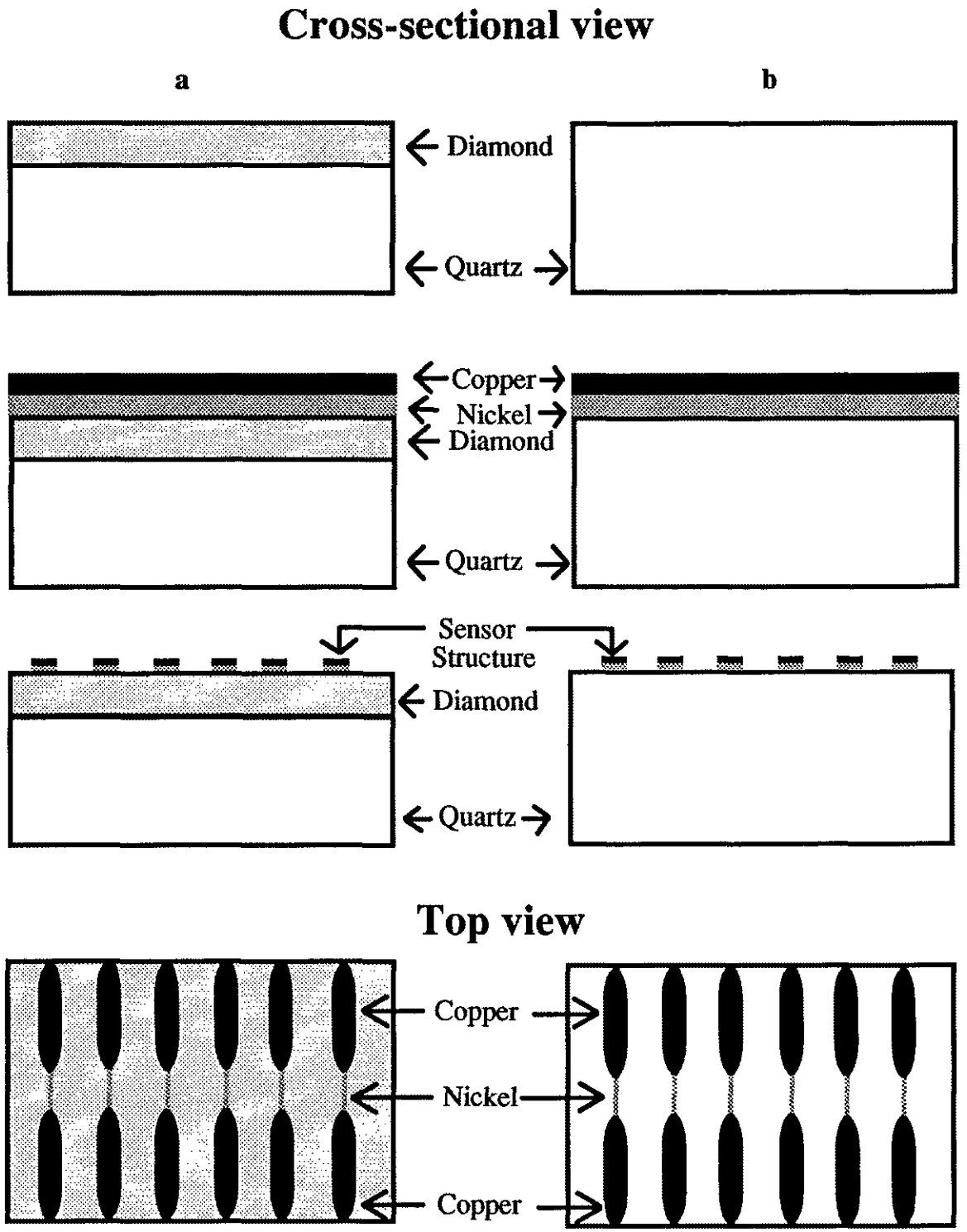

Figure 9: Sensor structures fabricated for frequency response tests
a) Ni/D/Q and b) Ni/Q sensors.

resistance values available [11]. Secondly, a thin film of copper was deposited onto top of the nickel film layer by the same evaporation technique. The purpose of the copper was to provide the electrical connection between the nickel sensor and the testing lead wire. A standard photolithographic technique was used for patterning both individual nickel sensors with lateral dimensions 100 μm x 1 mm and copper electrodes having surface dimensions of 1 mm x 1 cm. A wet chemical etching process involving sulfuric acid was used to remove the unwanted copper and nickel, leaving only the desired sensor structure geometry. A final wet chemical etchant was applied for selectively removing the copper metal from the sensor region. The thickness of the deposited nickel films was 0.25 μm on the quartz substrates and 0.5 μm on the diamond-on-quartz samples. The surface roughness of the diamond film made it necessary to deposit a thicker nickel film so that a continuous film would be formed. After fabrication, the completed sensor structures were then connected to a test board in the following manner. The bottom of each structure (Ni/Q and Ni/D/Q) was epoxied to an insulating surface. The insulating surface had copper pads deposited around the sensor structure, which served as electrical interconnection. Each copper electrode was soldered to lead wires which were subsequently attached to copper pads on the insulating surface. The copper pads on the insulating surface were then attached to a BNC connector. At this point, the sensors were ready for frequency response testing using an anemometer. Prior to discussing this testing procedure, it is essential to understand the operating principle of the anemometer, which is discussed in the next section.

4.2 Anemometry

Anemometers operate on the same principle as resistance transducers; the electrical resistance of a metallic conductor is a function of temperature. In fact, it is this principle which enables velocity fluctuations to be measured and interpreted as voltage changes. The sensing element (i.e. metallic conductor) used for anemometers come in two forms: hot-wires and hot-films. Hot-wire elements are typically made of tungsten, platinum, nickel, and their alloys, with an average diameter of 5 μm [34]. Due to the fragility of these probes, metal films deposited onto insulating substrates offer an advantage in mechanical strength. Also, there are two modes of operation for which anemometers are utilized: constant current and constant temperature. Comparisons of these two are discussed elsewhere [11] and since this research involved a constant temperature anemometer, the operation of only this type is briefly given.

4.2.1 Constant Temperature Anemometer Operation

The operation of a constant temperature anemometer has been studied extensively by various authors [35-40]. Prior to using the constant temperature anemometer to detect velocity fluctuations, a technique known as frequency optimization is done to establish the range for which a uniform frequency response is detectable. The frequency optimization technique as described by Freymuth [35,36] is very similar to the steps used for this research; therefore, a brief description of optimizing the CTA from this point of view is given. Figure 10 illustrates the schematic of a constant temperature anemometer, which consists of a square wave generator, a Wheatstone bridge and an amplifier. In this

configuration, the sensor is one arm of the Wheatstone bridge and placed in a variable current feedback loop which maintains a constant temperature. As a normal procedure, the system is placed in a flow environment in which the maximum flow velocity is known and an electrical signal is introduced into the bridge. The square wave is the closest electrical equivalent of a step change in velocity and allows for the adjustment of system stability. The initial temperature of the sensor is established by maintaining an overheat ratio, usually greater than one, between the variable resistor and the sensor. As a result, any resistance change of the sensor, corresponding to a temperature change, is detected as a voltage difference between the arms of the Wheatstone bridge. This voltage difference is electronically conditioned in stages and fed back as an input to the bridge. The electronic conditioning restores the original resistance (i.e. temperature) of the sensor by either increasing or decreasing the variable bridge voltage. Now, the voltage change which occurs at the top of the bridge is monitored and displayed to an oscilloscope. In particular, the rate at which the bridge voltage varies, such that the anemometer system reaches stability, is defined as the frequency response. Both a trimming condenser and a variable inductance are included within the anemometer system for properly tuning the system such that the maximum frequency response is obtained. Now, prior to actually optimizing the sensor in a flow environment, it is advantageous to estimate the frequency response in still air. This initial step gives experimenters useful information about the limitations of the sensor, which is important to know before scheduling a costly experiment. This standard procedure known as static electrical testing permits estimation of the sensor frequency response in a normal laboratory environment [41], and a good

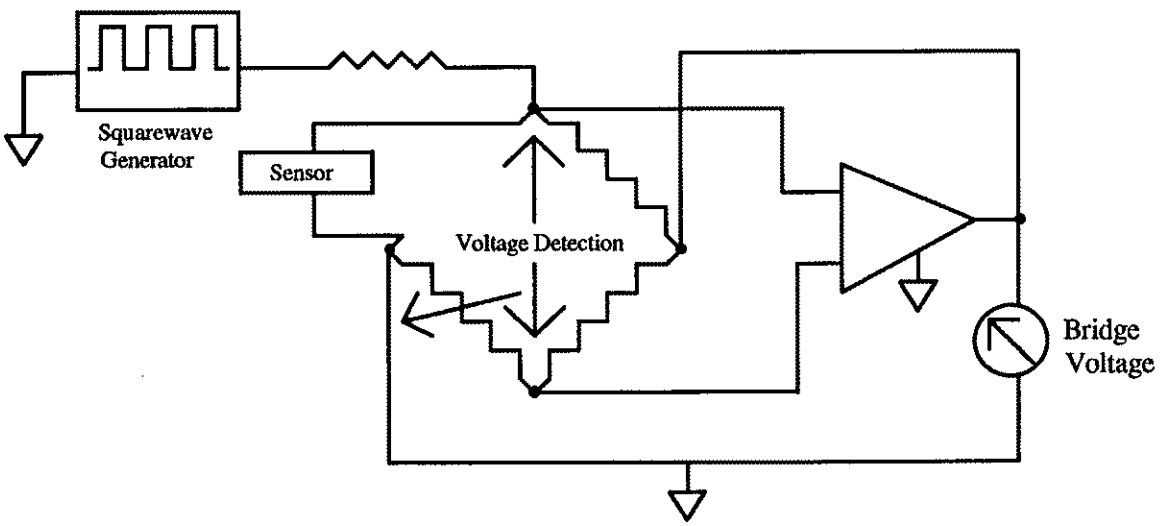

Figure 10: A schematic of the constant temperature anemometer.

correlation exists between this method and actual flow testing. This is done also by introducing an electrical square wave into the bridge followed by the same tuning steps described previously for optimizing the frequency response. The output of an optimized hot-film sensor using square wave testing is illustrated in Figure 11. The frequency response for this system is defined as $1/\tau$ [35].

4.3 Sensor Test Procedure

A Dantec Constant Temperature Anemometer (CTA) system [43] served as the primary tool for determining the frequency response. The main unit of the CTA model consists of: a servo amplifier, filter, decade resistance, square wave generator, and other auxiliary components. An associated CTA Standard Bridge and 5 meter Cable Compensation Unit were connected to the main unit of the CTA. The other equipment used during this test procedure included: Yokogawa 100 MHZ Digital Oscilloscope, Hewlett-Packard Multimeter, and 5 meter coaxial cable. The testing procedure began by first measuring and recording the resistance of each individual sensor in stagnant air; this value was defined as the "cold resistance." The resistance value measured was multiplied by a constant known as the overheat ratio. For all measurements, the overheat ratio was chosen to be 1.4. This overheat ratio was defined as the ratio of the control resistance to the sensor resistance at room temperature. Therefore, by multiplying the sensor "cold resistance" by the overheat ratio, the value for the control resistance was obtained. In practice, this meant setting the variable resistance of the Wheatstone Bridge equal to this multiplication result. A 3 kHz square wave signal from the anemometer was applied to the

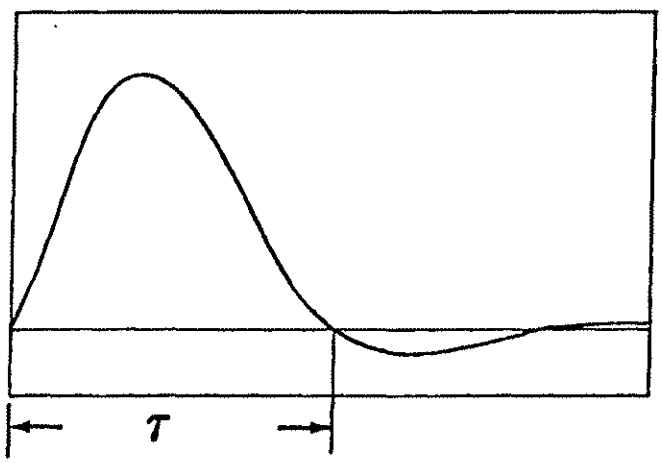

Figure 11: The frequency response of a hot-film anemometer (output voltage vs. time) due to electrical square wave testing [39].

sensor input and the resulting output was displayed on the digital oscilloscope. Adjustments were made to optimize the output waveform to look similar to Figure 11.

CHAPTER 5

RESULTS AND DISCUSSIONS

Diamond growth on quartz substrates was done using the nucleation techniques and growth parameters given in Chapter 3. Optical and scanning electron microscopes were used for characterizing the samples at different stages of the experiments. The uniformity of the surface abrasion technique was observed using the optical microscope, while characterization of the nucleation density and growth morphology was done with the SEM. Raman Spectroscopy was also utilized for characterizing the diamond quality. Nickel film sensors were patterned and deposited onto both diamond-on-quartz and untreated quartz samples. The frequency response of these sensors was measured using a constant temperature anemometer. This chapter presents the results and discussion of the diamond film synthesis first, followed by the frequency response analysis.

5.1 Diamond Film Synthesis

The surface pretreatment method involves abrading the quartz surface with a SiC paper and diamond paste combination using the Minimet polishing tool. The optical microscope reveals a surface with minute "scratches" occurring over the entire substrate. Figure 12 illustrates the SEM results using this nucleation method along with the

following growth parameters: 1000 W, 1% CH_4/H_2, 30 Torr, 950°C, and 6 hrs. As shown in Figure 12(a), the crystals are just now beginning to coalesce together with an approximate diameter of 5 μm. The crystal morphology appears to exhibit a random orientation growth pattern including (111) and (100) facets surfacing simultaneously on a single particle. Common to many of these crystals is a protruding corner of the (111) plane. Also, the nucleation density is approximately $1.0x10^6cm^{-2}$. It is apparent from Figure 12(b) that on certain areas of the substrate diamond growth did not occur and hence a thin film is not formed. Now, to see the effects of the surface abrasion technique, it is necessary to compare diamond growth on quartz without any surface pretreatment. Figure 13(a) reveals the results for an experiment conducted with similar growth conditions on an unabraded quartz substrate. The results shown here imply that the growth step alone is insufficient for obtaining an adequate nucleation density. Furthermore, by making a comparison with the results in Figure 12(b), it is proven that the surface abrasion technique can enhance the density of particles. The initial result of using gas phase seeding as the nucleation mechanism is shown in Figure 13(b). The deposition parameters are similar to those given previously, with a nucleation step of 5% CH_4/H_2 for 120 minutes as a precursor. This process is also suitable for initializing stable nuclei for diamond growth to develop; yet, the nucleation density is insufficient. Furthermore, the nucleation density within a given area for which crystal growth occurs appears to be higher for this experiment. As is expected, the growth morphology of these crystals closely resembles that shown in Figure 13(a). Since this morphology is not suitable for the desired thin films, adjustments were made in the nucleation procedure.

(a)

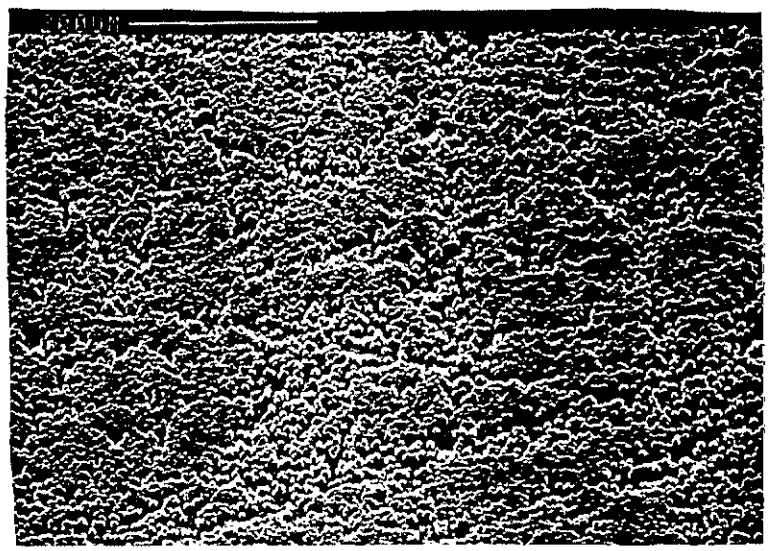

(b)

Figure 12: Diamond grown on quartz pretreated only with surface abrasion at (a) high magnification and (b) low magnification.

Modifications of the gas phase seeding step were attempted for increasing the nucleation density and changing the growth morphology, using a similar method previously reported [30]. The authors report a nucleation density of $2.0x10^6cm^{-2}$ for diamond growth on unscratched quartz substrates. Figure 14 illustrates the results of diamond growth for this present research using this method. The deposition parameters listed in Table 2 under the nucleation step were initially set up for a two hour seeding period. After the seeding period, the deposition parameters were modified for a four hour growth period as follows: 1000 W, 35 Torr, 865°C, and 1% CH_4/H_2. A significant change in the crystal morphology exists between the results here and those given in Figure 13(b). The crystallites shown here have a rounded geometrical shape and grow as hemispheres with tiny surface protrusions spontaneously occurring. At this stage, the crystals are beginning to merge or coalesce together and on some areas clustering is observed. Even though the density of particles is low, the change in crystal morphology from a protruding corner at the (111) plane to the rounded geometrical structure is significant toward obtaining the desired uniform thin films. The high percentage of CH_4/H_2 (14%) combined with reducing the microwave power, pressure and substrate temperature during the nucleation step collectively seem to effect the overall crystal morphology and size distribution when compared to the results in Figure 13(a). This is because the growth parameter which varied the most for the two experiments is substrate temperature. For a six hour deposition time the size of these crystals is significantly smaller; this is partly influenced by a reduction in plasma density due to the low microwave power. Since the

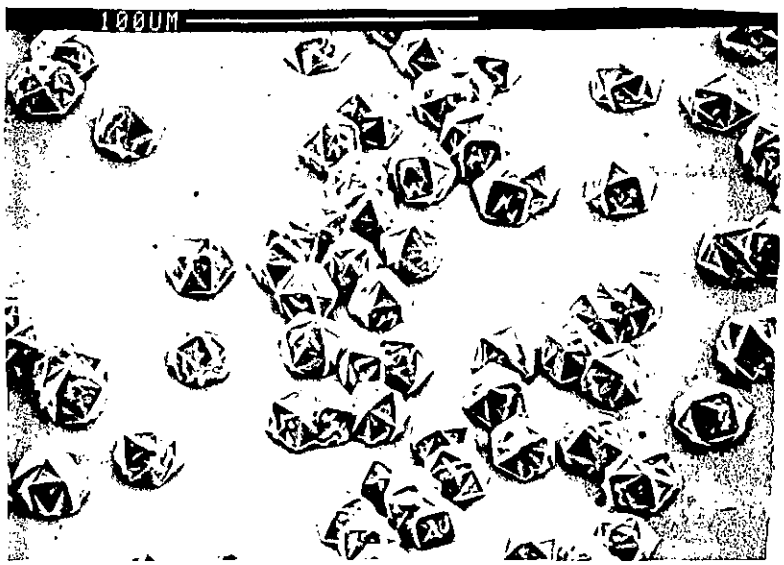

(a)

(b)

Figure 13: Diamond grown on quartz using similar growth conditions for (a) untreated without seeding (b) untreated with seeding.

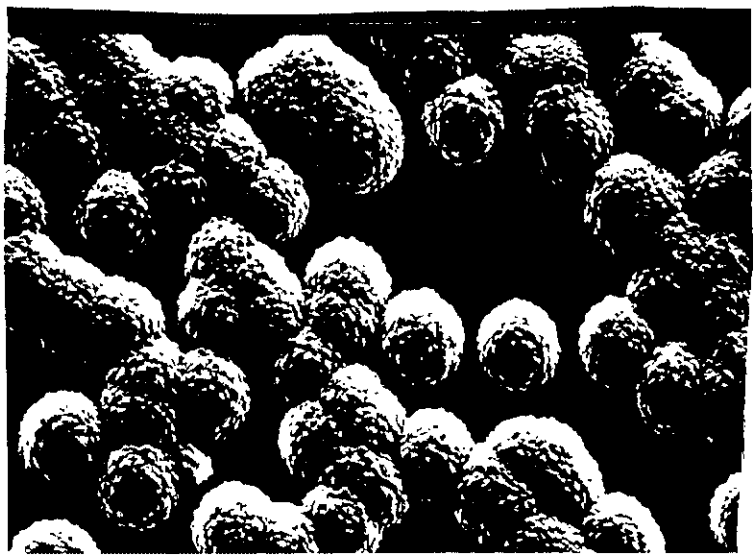

Figure 14: Diamond grown on untreated quartz with CH_4/H_2-14% gas phase seeding for 120 minutes.

nucleation density results were insufficient when the abrasive and nonabrasive methods were separately used, a combination of the two were investigated.

Figure 15(a) shows the results of applying both the abrasive and gas phase seeding technique as the nucleation mechanisms. The deposition parameters given in the preceding paragraph for the gas phase seeding and growth step were utilized during this experiment. Under similar deposition conditions the density of particles has tremendously increased such that a continuous film is formed. This is realized by the coalescence of the individual crystallites. Furthermore, the particle size distribution appears almost uniform within the entire region. Also, carbon monoxide at 3% was added during the growth step to enhance the diamond quality. Diamond growth without CO is shown in Figure 15(b). By comparison, the growth morphology is similar to that shown in Figure 15(a). Therefore, the combination of surface abrasion and gas phase seeding effectively enhance the nucleation density and as a result a continuous thin film is grown.

Raman spectra of a natural diamond and for diamond growth on untreated quartz substrate (Figure 14(a)) is illustrated in Figure 16. The peak intensity of the natural diamond is at 1332 cm^{-1}, shown in Figure 16(a); while, the peak intensity is shifted to in Figure 16(b). The results illustrated in Figure 17 show a comparison between thin film growth with and without CO. Clearly, the intensity of the diamond peak is more pronounced for the experiment with CO. The shift from the normal 1332 cm^{-1} peak can be due to several factors such as sp^2 bonding occurring during the gas phase seeding step or the stress state of the films caused by the thermal expansion mismatch. This agrees with other results of diamond growth on hard substrates which show Raman bands and peaks

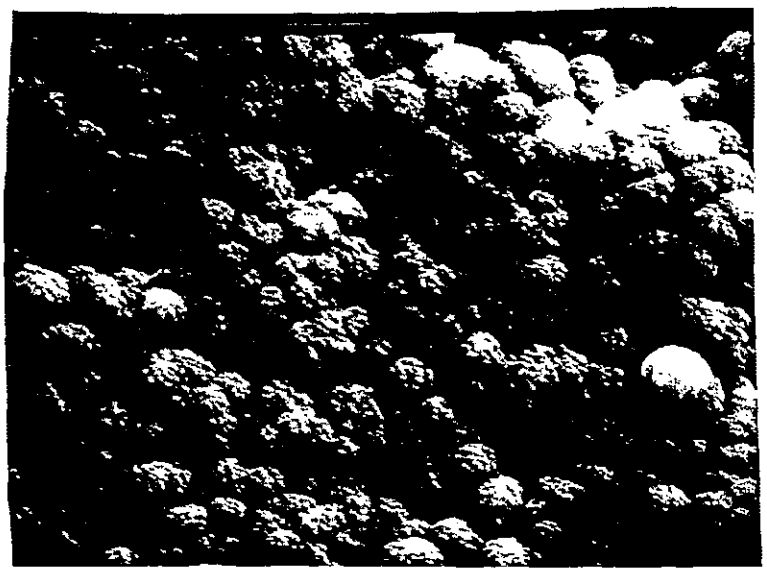

(a)

(b)

Figure 15: Diamond growth on quartz with CH_4/H_2-14% gas phase seeding (a) with CO and (b) without CO.

which shift in wavenumber [44]. The broadband peak at 920 cm^{-1} can be a result of SiC formation, which has been detected for diamond growth on quartz [28]. The intensity of the normal broad peak from 1500-1550 cm^{-1} which corresponds to amorphous carbon is smaller when CO is present. The quality of diamond is qualitatively determined by the intensity ratio of the first order line to this broad band. The intensity ratio of the diamond thin films grown with CO is much greater than the film grown without CO. Comparing Figure 17(a) and Figure 16(b) shows that the addition of CO has the effect of maintaining high quality diamond.

The nucleation density is greatly enhanced when the combination of surface pretreatment and gas phase seeding is done. Surface abrasion can cause an immediate means of nucleation by seeding stable fragments on which diamond growth can occur. Gas phase seeding allows carbon species to impinge upon the surface and subsequent diffusion into the bulk of the substrate. As a result, the creation of a large density of stable nuclei is formed, hence uniform thin film growth will occur. The crystal morphologies presented here are similar to other reports in which low methane concentrations yield faceted crystals and higher methane concentrations produced rounded crystallites [26]. The desired uniform thin film was obtained by modifying the gas phase seeding process with increasing methane concentration, while simultaneously decreasing the microwave power, substrate temperature and pressure.

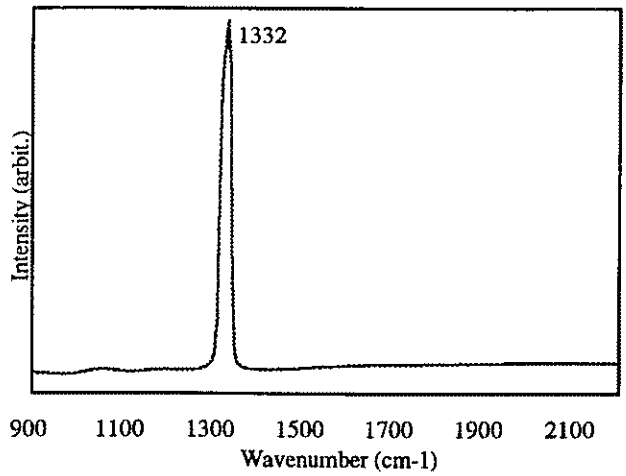

(a)

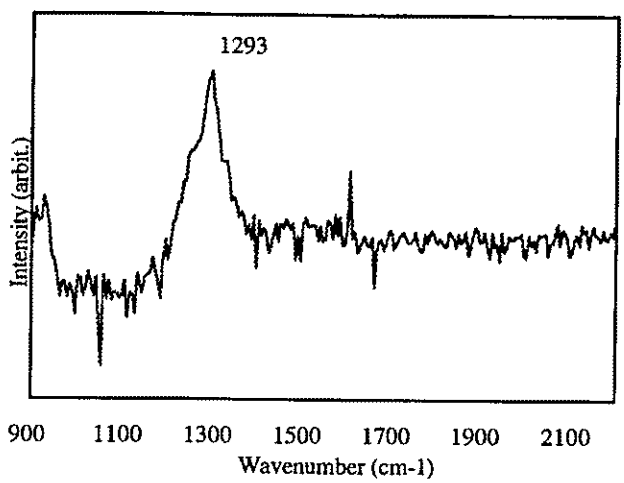

(b)

Figure 16: Raman spectra of (a) natural diamond (b) diamond crystals grown on untreated, unseeded quartz, as shown in Figure 14(a).

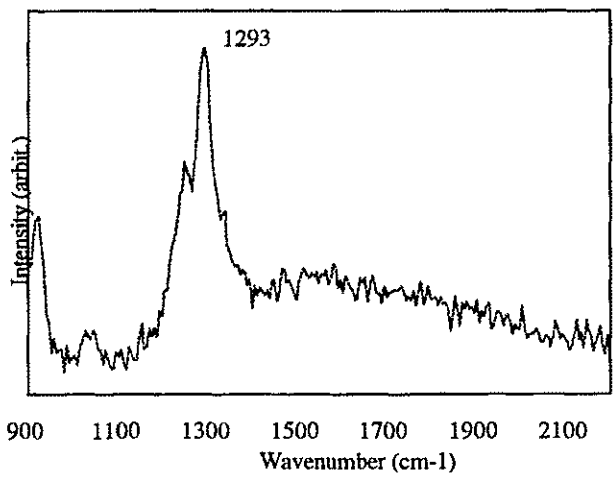

(a)

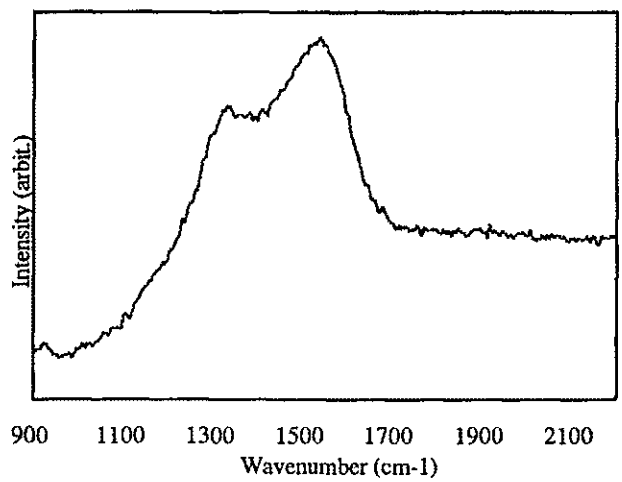

(b)

Figure 17: Raman spectra of diamond films grown on quartz substrates pretreated by surface abrasion and gas phase seeding (a) with CO (b) without CO.

5.2 Frequency Response Analysis

The frequency response for the conventional metal sensor (Ni/Q) and the diamond enhanced sensor (Ni/D/Q) is illustrated in Figures 18 and 19. The frequency response is defined as $1/\tau$, where τ is the pulsewidth in microseconds. The response for the Ni/Q sensor is 100 kHz, which is representative of a typical metal film sensor. The frequency response of the diamond enhanced sensor is around 240 kHz. As stated previously, the Ni/D/Q sensor has a film thickness twice the value of the Ni/Q sensor. According to the theoretical calculations presented in section 2.1, the frequency response is a function of the inverse of the square of the film thickness. However, the frequency response of the Ni/D/Q sensor is more than double the value of the conventional sensor. Therefore, even with a thicker metal film an interlayer of diamond between the metal film and substrate enhances the frequency response.

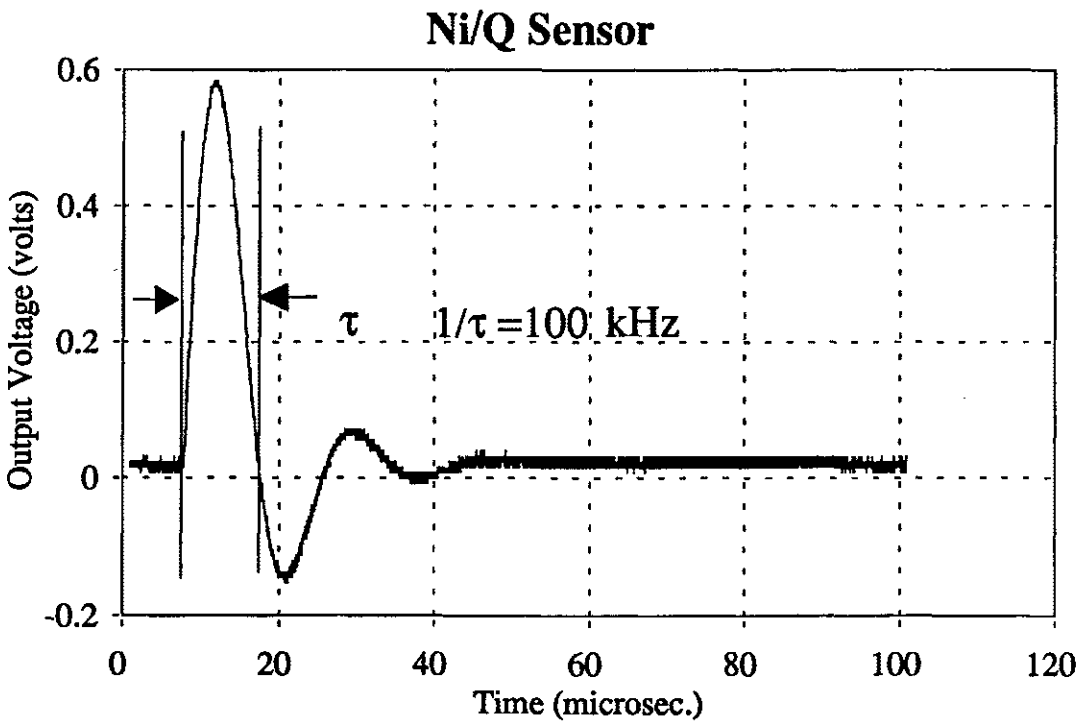

Figure 18: Frequency response of a conventional metal film sensor.

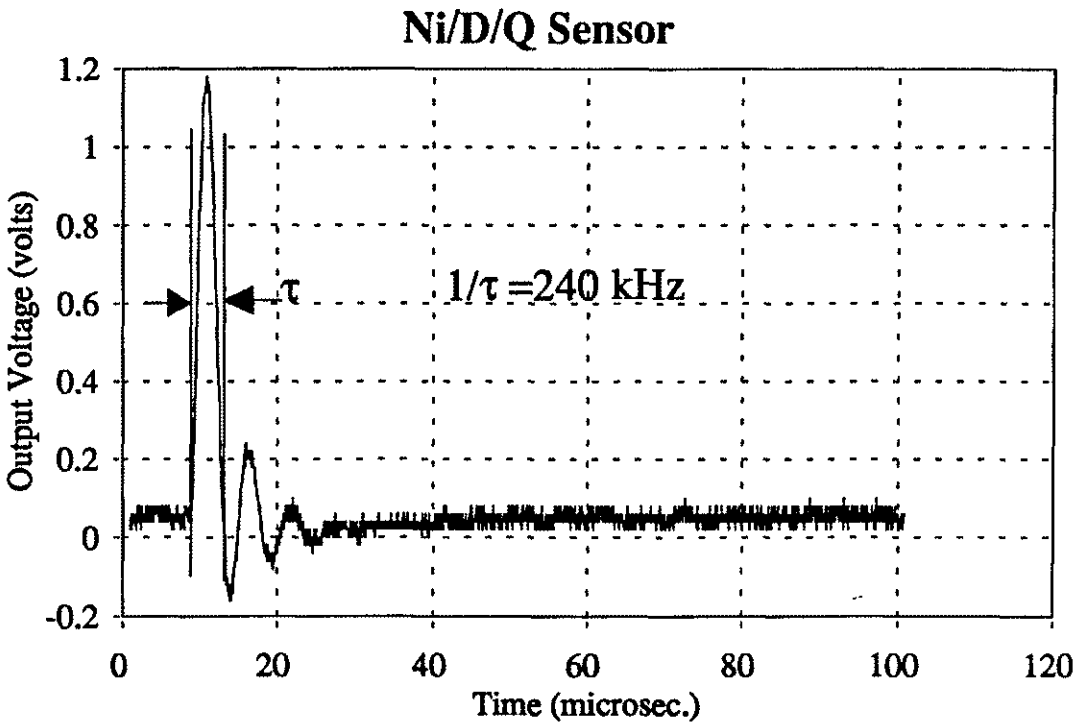

Figure 19: Frequency response of a diamond enhanced sensor.

CHAPTER 6

SUMMARY AND CONCLUSION

A constant temperature anemometer is a useful tool for measuring boundary layer transitions in supersonic and hypersonic speed regimes. The sensing probes are fabricated in the form of a thin film deposited onto an insulating substrate. Thin films offer the advantage of being mechanically strong and maintaining a large signal-to-noise ratio. The frequency response of the sensors in high velocity environments is expected to be in the 200-400 kHz range. Thin film sensors fabricated previously have been limited to 100 kHz as the useable range. Inserting a diamond film between the metal film and substrate is investigated for increasing the frequency response.

6.1 Theoretical Analysis

Theoretical calculations have determined that the maximum frequency response is related to $k_f/\rho_f c_f d^2$, where k, ρ, c, and d are the thermal conductivity, density, specific heat capacity and thickness of the film, respectively. This is achieved by maintaining a high ratio of the film thermal conductivity to the substrate thermal conductivity ($k_f \gg k_s$). Diamond emerges as having the largest value of thermal conductivity among solid state materials at room temperature. Growing high quality diamond films using different

chemical vapor deposition techniques on a variety of substrates has been achieved. Quartz emerges as a suitable substrate material for maintaining a high (k_f/k_s) ratio. Theoretical studies have shown that an intermediate layer of diamond between a metal film and a substrate can reduce the temperature of the metal film. As a result, the effective thermal conductivity of the metal film can be increased by inserting diamond between the metal and substrate. Numerical calculations were done previously in our group using the finite-difference method for computing the frequency response of two sensor structures: a conventional metal film sensor (Ni/Q) and a proposed diamond enhanced sensor (Ni/D/Q). The 3dB normalized temperature amplitude response of the diamond enhanced sensor is approximately $3x10^5$ Hz. However, the conventional sensor yielded a response about an order of magnitude lower. Consequently, the proposed diamond enhanced sensor should experimentally have a frequency response higher than a conventional sensor. The two types of sensors were fabricated in order that comparative frequency response measurements could be done.

6.2 Diamond Film Synthesis

Fabricating the diamond enhanced sensor began by determining the nucleation and growth parameters for diamond thin film growth on quartz. Diamond growth was conducted in a microwave plasma enhanced chemical vapor deposition (MPECVD) system. Two techniques, surface abrasion and gas phase seeding, when used separately have been shown to increase the nucleation density for diamond growth. For this research, the combination of surface abrasion and gas phase seeding were necessary to

obtain the desired uniform thin films, which was diamond growth with a minimum amount of surface roughness. Modifying the gas phase seeding technique with a high methane/hydrogen ratio was a crucial step in decreasing the surface roughness. However, increasing the methane concentration also increases the formation of non-diamond growth particles. As a result, the addition of carbon monoxide during the growth step was needed to obtain high quality diamond films.

6.3 Fabrication and Testing

Nickel film sensors were deposited onto both quart and diamond-on-quartz substrates by e-beam evaporation. A thin film of copper was subsequently deposited, and served as the electrical connection between the sensor and the testing wire. The thickness of the nickel films deposited on the diamond-on-quartz substrates was two times greater than the nickel films deposited onto quartz. Standard photolithography was used to pattern the deposited metal into the desired sensor geometry. The sensors were connected to a test board for frequency response measurements. A constant temperature anemometer was utilized to determine the frequency of both the conventional metal film and the diamond enhanced sensor. The sensor is one arm of a Wheatstone bridge in the anemometer configuration. A technique known as static electrical testing was done for evaluating the frequency response in a laboratory environment. An electrical square wave was introduced into the bridge, and the corresponding output waveform was displayed on an oscilloscope. The output represented the rate at which the bridge voltage varied until the anemometer system reached stability. This was defined as the frequency response and

was shown to be equivalent to $1/\tau$, where τ is the pulsewidth. The frequency response of the diamond enhanced sensor was 240 kHz. The conventional sensor yielded a frequency response of 100 kHz, which is standard for this type. Since the thickness of the metal films for the conventional sensor is one-half as thick as the metal films used for the diamond enhanced sensor, it is quite clear the interlayer of diamond enhances the frequency response.

6.4 Future Work

The actual value of the thermal conductivity for the diamond films was not measured. The thermal conductivity value of diamond as well as the effective diffusivity value for the nickel/diamond combination could experimentally be determined. The actual themal conductivity value is important for validating the theoretical sensor model. The theoretical frequency response calculated using the finite-difference method for the diamond enhanced sensor was $3x10^5$ Hz. This calculation was done for a one-dimensional case where the thickness of the nickel and diamond films were 50 μm each. The thickness of the nickel and diamond films used in this research were 0.5 μm and 6 μm, respectively. The frequency response for the diamond enhanced sensor was 240 kHz. A more comprehensive three-dimensional model could be developed for analyzing the dimensions of this sensor.

The frequency response for these sensors was obtained in a laboratory environment. Testing could be done for determining the actual frequency response in a wind tunnel environment. Other work could involve growing doped diamond thin films

onto quartz. Doping enables the diamond films to become electrically conductive. By doing so, the existing problem of surface roughness for nickel film deposition can be eliminated and the diamond film could become the sensor.

REFERENCES

[1] F.K. Owens, AIAA Paper 90-5231, 1990.

[2] R.B. Miles, J. Connors, E. Markovitz, P. Howard, and G. Roth, Phys. Fluid A, 1, 389, 1989.

[3] F.P. Incropera and D.P. DeWitt, Fundamentals of Heat Transfer, Chapter 6, John Wiley & Sons, Inc., New York, 1981.

[4] H.H. Lowell, Advances in Hot Wire Anemometry, eds. W.L. Melnik and J.R. Weske, 1968.

[5] R.B. Belser, and W.H. Hicklin, J. Appl. Phys., 30, 313, 1959.

[6] B.J. Bellhouse and D.L. Schultz, J. Fluid Mech., 24, 379, 1966.

[7] G.L. Brown, Proc. Of the 1967 Heat Transfer and Fluid Mechanics Institute, Stanford Press, 362, 1967.

[8] M. Acharya, Rev. Sci. Instrum., 50, 952, 1978.

[9] E. Gartenburg, M.A. Scott, S.D. Martinson, and S.Q. Tran, Fourth Triennial International Symposium on Fluid Control, Measurements and Visualization, France, 1994.

[10] C.B. Johnson, D.L. Carraway, P.C. Stainback and M.F. Fancher, AIAA Paper 87-0049, AIAA, New York, 1987.

[11] V.A. Sandborn, Resistance Temperature Transducers, Metrology Press, Colorado, 1972.

[12] B.V. Spitsyn, Materials Research Society International Conference Proceedings 1991, 909, 1991.

[13] W.P. Kang, Y. Gurbuz, J.L. Davidson, and D.V. Kerns, J. Electrochem. Soc., 141, 2231, 1994.

[14] M. Aslam, et.al., Diamond Film Semiconductors, SPIE, 2151, 145, 1994.

[15] C. Ellis, D.A. Jaworske, R. Ramesham, and T. Roppel, Technical Digest of the IEEE Solid-State Sensor and Actuator Workshop, Hilton Head Island, SC, 132, 1990.

[16] S. Matsumoto, Y. Sato, M. Tsutsum, and N. Setaka, J. Mater. Sci., 17, 3106, 1982.

[17] J.C. Angus and C.C. Hayman, Science, 241, 913, 1988.

[18] P.K. Bachman and R. Messier, C&EN, 67, 24, 1989.

[19] N. Setaka, Synthetic Diamond: Emerging CVD Science and Technology, eds. K.E. Spear and J.P. Dismukes, John Wiley & Sons, Inc., New York, 1994.

[20] S. Albin, W.P. Winfree, B.S. Crews, J. Electrochem. Soc., 137, 1973, 1990.

[21] L.I. Maissel and R. Glang, Handbook of Thin Film Technology, Chapter 6 McGraw-Hill, 1970.

[22] J.S. Tsacoyeares and T. Feng, SPIE Proceedings: Diamond Optics, eds. A. Feldman and S. Holly, 969, 186, 1988.

[23] R.J. Vidal, WADC Tech Note 56-315, AD-97238, 1956.

[24] B. Bulusu, Diamond Thin Film Sensors For Hypersonic Flow Studies, Master's Thesis, Old Dominion University, 1994.

[25] S. Albin, B. Bulusu, S.D. Martinson, D.S. Gray, Thermal Anemometry, 167, 181, 1993.

[26] K. Kobashi, K. Nishimura, Y. Kawate, T. Horiuchi, Phys. Rev B, 38, 4067, 1988.

[27] S.D. Wolter, B.R. Stoner, J.T. Glass, Appl. Phys. Lett., 62, 1215, 1993.

[28] D.J. Pickrell, W. Zhu, A.R. Badzian, R.E. Newham, R. Messier, J. Mater. Res., 6, 1264, 1991.

[29] F.S. Lauten, Y. Shigesato, B.W. Sheldon, Appl. Phys. Lett., 65, 210, 1994.

[30] P.E. Pehrsson, F.G. Celii, J.E. Butler, in Diamond Films and Coatings, ed. R.F. Davis, Noyes Publications, New Jersey, 1993.

[31] Y. Muranaka, H. Yamashita, H. Miyadera, Thin Solid Films, 195, 257, 1991.

[32] P. Freymuth, Rev. Sci. Instrum., 38, 677, 1967.

[33] S.M. Sze, VLSI Technology, 2nd ed., McGraw-Hill, New York, 1988.

[34] A.E. Perry, Hot-Wire Anemometry, Oxford University Press, New York, 1982.

[35] P. Freymuth, J. Phys. E: Sci. Instrum., 10, 705, 1977.

[36] P. Freymuth, J. Phys. E: Sci. Instrum., 11, 177, 1978.

[37] P. Freymuth, J. Phys. E: Sci. Instrum., 14, 238, 1981.

[38] A.E. Perry and G.L. Morrison, J. Fluid Mech., 47, 577, 1971.

[39] J.P. Bonnet and T.A. de Roquefort, Rev. Sci. Instrum., 51, 234, 1980.

[40] J.A. Borgos, TSI Quarterly, 6 , 3, 1980.

[41] M.A. Scott, Aerospace Technologist, NASA Langley, private communication.

[42] Dantec Reference Manual for Constant Temperature Anemometers, 1985.

[43] C. Wild, N. Herres, P. Koidl, J. Appl. Phys., 68, 973, 1990.

[44] D.S. Knight and W.B. White, J. Mater. Res., 4, 385, 1989.